

## HEAT RELEASE MECHANISMS IN INHIBITED LAMINAR COUNTERFLOW FLAMES

**Ki Yong Lee, Don J. Cha, and Ishwar K. Puri**  
Department of Mechanical Engineering  
University of Illinois, Chicago  
Chicago, Illinois

**Anthony Hamins,**  
Building and Fire Research Laboratory  
National Institute of Standards and Technology  
Gaithersburg, Maryland

### ABSTRACT

Both the chemical kinetic and thermal channels of inhibition must be simultaneously characterized in order to understand the effectiveness of chemical agents on flame stability. However, due to the participation of inhibitors in flame chemistry, it is difficult to concurrently characterize the complex interaction between their cooling action, and the chemical kinetic effects due to them. Investigations involving chemical inhibitors have to contend with three interacting phenomena, i.e., (Chang et al., 1987) the cooling action due to the specific heat of the species; (Karra et al., 1988) the heat release due to their burning; and (Pitz and Westbrook, 1990) inhibition associated with scavenging of critical radical species. This study investigated the effect of chloromethane (a chemical inhibitor) on the heat release in methane-air nonpremixed flames. For comparison, the effect on the heat release due to the purely thermal action of nitrogen was also investigated. The flames were experimentally and numerically studied in a counterflow configuration, and the heat release was calculated from simulations involving detailed chemistry. When inert suppressants were added to the oxidizer stream of a nonpremixed flame, the global heat release decreased. Chloromethane addition to the fuel stream, however, increased the heat release. Whereas addition of nitrogen narrowed the heat release region, chloromethane addition to the oxidizer altered the flame stoichiometry, such that the heat release profiles were markedly different. A thorough investigation of flame stability must consider the importance of heat losses through radiative emission. Halogenated compounds can influence flame emission through changes in flame structure including increases in temperature and soot

concentration. For these reasons, a small Schmidt-Boelter type gauge was used to measure the radiative flux through a cylindrical control volume surrounding the flame, and the total radiation emitted from the flame was calculated by integrating the emitted flux. The results show that as nitrogen was added to the methane-air base flame, the radiative heat loss fraction decreased slightly. When chloromethane was added to the oxidizer stream, the radiative heat loss fraction increased substantially ( $\approx 40\%$ ). Values of the radiative heat loss fraction remained relatively unchanged ( $\approx 2-3\%$ ) for all of the flames studied.

### INTRODUCTION

To better understand the mechanism of flame inhibitors, both the kinetic and thermal channels of inhibition must be simultaneously characterized. From the perspective of flame stability, it is important to identify the influence of chemical agents on flame heat release. Flame extinction occurs when heat losses exceed heat generation. For instance, thermal inhibitors cool flames through heat capacity effects, whereas chemical inhibitors simultaneously cool flames and reduce radical superequilibrium concentrations.

Fundamental investigations of chemical inhibitors are necessarily limited to those substances whose participation in hydrocarbon chemistry is relatively well characterized by detailed chemical kinetic mechanisms. Chemical inhibitors for which detailed chemical kinetic information is available are the simpler halogenated hydrocarbons such as chloromethane (Chang et al., 1987, Karra et al., 1988, Pitz and Westbrook, 1990, Barat et al., 1990). Simple halogenated species react with oxygen at high temperatures.

behaving not unlike fuels. Thus, investigations involving halogenated agents have to unravel three interacting phenomena, i.e., (Chang et al., 1987) cooling due to the specific heat of the species; (Karra et al., 1988) heat release due to their burning; and (Pitz and Westbrook, 1990) scavenging of critical radical species. These interactions are complex and are coupled.

The inhibition of critical radical species due to thermal and chemical inhibitors has been the focus of an earlier investigation in our laboratories (Yang et al., 1994). In that study, attention was focused on the detailed temperature, species, and velocity profiles in inhibited flames. Velocity and temperature measurements in the counterflow flames were used to validate the computational flame model (Yang et al., 1994, Huh et al., 1994, Yang and Puri, 1993). In the study that we report here, attention was focused on the heat release and its form, in both inhibited and non-inhibited counterflowing flames.

A thorough investigation of flame stability must consider the importance of heat losses through radiative emission. Halogenated compounds can influence radiative emission through changes in flame structure including increases in the temperature field and soot concentration. Inherent in nearly all calculations involving counterflow flames has been the assumption that radiative emission from the flame is negligible. Non-negligible radiative emission will impact the temperature and species profiles determined from the numerical models. Concern about the issue of radiative loss near extinction in nonpremixed counterflow flames prompted the development of an asymptotic theory of flame structure that includes thermal radiation (Sohrab et al., 1982). In that study radiative losses were considered to be relatively small compared to the heat release established at conditions near extinction. In a separate study, the radiative heat transfer from a "cylindrical" counterflow flame was determined by integrating the heat and mass transfer equations using measured flame structure data and estimated soot volume fractions (Abdel-Khalik et al., 1974). Recently, detailed radiative emission calculations that include contributions due to both particulates and gas band emission in counterflow flames have been reported (Hall, 1993, Vranos and Hall, 1993, Chan et al., 1993). The flames involving chloromethane studied here, are characterized by a yellow luminosity, calling into question the relative importance of thermal radiation in the simulations (Yang et al., 1994, Huh et al., 1994). Thus, measurements are made to determine the magnitude of radiative losses from these counterflow flames.

Counterflow flames result when two axisymmetric reactant streams flow towards each other in a stagnation point flow. These flames are well suited for the investigation of flame structure since the stretch rate, which defined the flowfield, is an independently controlled parameter. In the case of laminar flows, the resulting flame structure is steady and one-dimensional with respect to temperature and species concentrations. The structure of

counterflowing flames has been extensively studied using numerical codes which integrate the conservation equations and include detailed models of molecular transport and chemical kinetics (Dixon-Lewis et al., 1984, Smooke and Giovangigli, 1991, Rogg, 1991). Use of these models has focused on a number of applications including flame stability and pollutant formation. A wide variety of fuel types (methane, chloromethane, heptane, hydrogen, to name a few) and flame configurations (nonpremixed, partially premixed, and premixed) have been investigated. Therefore, these flames are attractive from the perspective of investigating flame inhibition phenomena.

## OBJECTIVES

The objectives that motivated this investigation are listed below.

1. The effect of inhibitors on the structure of hydrocarbon flames was the focus of study to gain insight into the complex interactions that impact the global heat release in flames and, ultimately, flame stability, since chemical inhibition may manifest itself through decreases in key radical species concentrations, alteration of the flame heat release profiles, and/or by changes in radiative emission.
2. A second objective was to develop a methodology for the measurement of radiative emission from counterflowing flames, and to compare the impact of suppressants on the radiative heat loss emitted from a flame.

## METHODOLOGY

Laminar counterflow flames established under atmospheric conditions were investigated. An uninhibited methane-air "base" flame was compared with flames that were inhibited by adding molecular nitrogen and chloromethane to the oxidizer stream. In one additional case, chloromethane was added to the fuel stream. Nitrogen behaves as a thermal inhibitor when added to flames, whereas chloromethane has a combination of physical and chemical behavior (Yang et al., 1994). The physical behavior of  $N_2$  is manifest by its thermal cooling of flames, causing a decrease in key reaction rates which impact the heat release. Therefore, no significant differences are to be expected if nitrogen is added to either the fuel or oxidizer stream as long as "accessibility" to the flame is considered. In contrast,  $CH_3Cl$  exhibits different chemical kinetic behavior when added to the fuel or oxidizer stream due to the reactivity of chloromethane. When  $CH_3Cl$  is added to the oxidizer stream, inhibition effects are due to the formation of a premixed type reaction zone, whereas addition of this species to the fuel stream involves combustion of a nonpremixed flame with two initially distinct fuels. In the study reported here, chloromethane

addition to the fuel stream of a methane-air flame was also investigated.

### Chemistry-flow interaction

The coupling that exists between a flame and the flowfield is of fundamental importance to combustion processes. One flame-flowfield interaction is the response of a flame to a straining flowfield. This is often characterized through a single parameter, i.e., the Damköhler number (Williams, 1985). In counterflowing streams, a flame is established at a fixed fluid dynamic stretch rate and the reactant composition can be changed to investigate effects that arise due to the flame chemistry (Yang et al., 1994). Therefore, for each flame discussed here, the stretch rate was maintained constant to analyze significant elements of the inhibition-related chemistry in equivalent flowfields. Since there are distinct stretch rates corresponding to different regions in a flame, the stretch rate referred to here is the gradient of the axial velocity on the oxidizer side of the high temperature reaction zone (Yang et al., 1994, Huh et al., 1994, Chelliah et al., 1990).

### Burner

Atmospheric laminar counterflow flames were established in a burner that has been previously described (Yang et al., 1994). Disturbances due to radiative flux transducers positioned inside the ducts were minimized by increasing all burner dimensions by a factor of 2.0 from those reported in Refs. (Yang et al., 1994, Huh et al., 1994, Yang and Puri, 1993). The burner consisted of two opposed ducts placed 15 mm apart. The ducts, with a 48 mm inner diameter, contained several fine wire mesh screens near the duct exits, a standard technique causing the flow to be laminar (Hamins et al., 1985, Puri, 1987). The reactant streams were metered through calibrated flowmeters. A co-annular flow of nitrogen isolated the flames from ambient disturbances. The diameter of the visible flames, upon introduction of the nitrogen curtain, was 82 mm in all cases.

### Conditions

Oxidizer-side inhibition: Measurements showed that at a stretch rate corresponding to  $\approx 98 \text{ s}^{-1}$ , 14.1 % (by volume) nitrogen or 9.6 % chloromethane must be added to the oxidizer stream of the methane-air flame to extinguish it. Five flames established at a stretch rate of  $98 \text{ s}^{-1}$  were investigated including (1) a methane-air "base" flame; and the methane base flame inhibited by addition of (2) 6.6% excess nitrogen (by volume), (3) 13% excess nitrogen, (4) 5% chloromethane; and (5) 9% chloromethane. Flames (1)–(3) were visibly blue indicating the absence of a substantial amount of soot, whereas flames (4) and (5) were

yellowish on the fuel side and blue on the oxidizer side of the high temperature reaction zone. Flame (1) represented vigorous burning conditions. Flames (3) and (5) were close to extinction, whereas flames (2) and (4) were established at conditions intermediate between vigorous burning and extinction.

Fuel-side inhibition: A flame with 50% chloromethane by volume added to the fuel stream extinguished at a critical stretch rate corresponding to  $\approx 160 \text{ s}^{-1}$ . Therefore, a sixth inhibited flame with 50%  $\text{CH}_3\text{Cl}$  by volume added to the fuel stream of the methane-air flame was also established at a stretch rate of  $\approx 98 \text{ s}^{-1}$ , i.e., relatively close to extinction.

### Numerical method

Numerical simulations of strained nonpremixed flames were performed using a previously developed computer code (Rogg, 1991) that employs a detailed model of the molecular transport of chemical species, as well as detailed chemical reaction schemes (Rogg, 1989). The chemical kinetic scheme was taken from the literature (Barat et al., 1990, Miller and Bowman, 1989). The kinetic mechanism includes 357 elementary forward and backward reactions, and involves 38 gas-phase species, including  $\text{C}_2$  chlorinated and non-chlorinated hydrocarbons. Further details of the calculation methodology are described in Refs. (Yang et al., 1994) and (Lee et al., 1994). For convenience, the reaction numbers referred to here correspond to those employed previously (Yang et al., 1994, Lee et al., 1994).

### Radiation

The radiative heat loss fraction  $\chi_R$  is the ratio of the radiative emission from a flame  $Q_{rad}$  taken with respect to the combustion heat release rate  $Q_{chem}$ .  $\chi_R$  values on the order of 0.01 to 0.06 have been predicted depending on the global flow field strain rate in high pressure and atmospheric counterflowing methane-air nonpremixed flames (Vranos and Hall, 1993, Chan et al., 1993). For a steady nonpremixed flame in a typical configuration, such as that involving a pool or jet,  $\chi_R$  is experimentally determined by measuring the mass burning rate and the radiative heat loss through a control surface surrounding the flame (McCaffrey, 1981, Hamins et al., 1991). In jet flames  $\chi_R$  depends on both fuel type and total heat release. Methane jet flames, for example, have  $\chi_R$  values between 0.05 and 0.30 for 5 to 70 kW heat release flames (McCaffrey, 1981).

The radiative heat flux emitted by the flames was measured using a small water-cooled Schmidt-Boelter gauge at locations on a cylindrical control surface surrounding the flame. The gauge had a 6.35 mm outer diameter, a flat spectral response, and a view angle of  $150^\circ$ . The transducer

was calibrated using a tungsten lamp and a reference gauge traceable to NBS standards. A hole was cut into the screens to accommodate the transducer which was inserted into either duct such that its face was flush with the screens. The gauge was water cooled with a tube extracted through the base of the ducts. A schematic diagram of the burner and measurement assembly is presented in Fig. 1. Under conditions of high radiative heat flux, heat transfer from the gauge face to a passing fluid is possible due to high temperature of the gauge face. Non-combusting experiments with an infrared heat lamp showed that convective transfer from the face of the gauge to the reactant streams was negligible. An uncertainty estimate of 10% for the radiative flux measurements was determined from an error analysis.

### Radiative heat flux measurements

The gauge was placed at the periphery of the control volume as shown in the schematic diagram presented in Fig. 2. For certain cases, when the transducer was placed inside either duct, it was observed to visibly distort the flame. For these situations, the transducer and screens were moved back inside the duct until the malformation disappeared. Two typical displacement values, of 5.3 mm (Case I), and 12.8 mm (Case II), were found sufficient to provide undisturbed flames for the conditions investigated. These cases are illustrated in Fig. 2. Measurement of the radiative flux to the plane of the duct were made at the centerline of symmetry and at two radial positions (12.7 and 41 mm). Since the measurement location at 41 mm from the axis of symmetry was outside the duct, introduction of the transducer at that station had a negligible effect on the flowfield, allowing placement of the transducer face flush with the duct exit plane. Measurements of radiative emission from the sides of the cylindrical control volume were made at 21 vertical locations at a distance  $R_3$  ( $= 60$  mm) with the gauge oriented towards the axis of symmetry. The flow and measurement conditions are listed in Table 1.

### Radiative heat flux corrections

Measurements made with the transducer placed in the duct interior were corrected to obtain the heat flux out of the control volume, i.e., at the duct exit plane (see Fig. 2). All of the emitted radiation was assumed to originate from the surface of the visible flame zone which was modeled as a radiating disk. Configuration factors obtained from Ref. (Howell, 1982) were employed. This assumption is reasonable, since effects due to flamelet thickness on thermal radiation are important only for flames at low strain rates (Hall, 1993). In addition, since no significant radiative absorption occurred due to methane, air-nitrogen, or air-chloromethane mixtures, a view factor correction was suitable. The moderate strain rate at which the flames were investigated was motivated in part to obtain sufficiently

optically thin flames to which application of the configuration factor correction was appropriate.

The experimental control volume was defined as a cylinder 120 mm in diameter and 15 mm in length. When the transducer was embedded inside the duct on the axis of symmetry, the relevant configuration factor was that of a disk parallel to a coaxial disk of unequal radius (Howell, 1982):

$$F_{1,2} = 0.5 [X - \sqrt{X^2 - 4(R_1/R_2)^2}] \quad (1)$$

where  $F_{1,2}$  denotes the configuration factor,  $R_1$  and  $R_2$  respectively equal  $(r_1/h)$  and  $(r_2/h)$  (with  $r_1$  and  $r_2$  representing the radii of the visible flame and the transducer, respectively, and  $h$  the distance between the transducer and the visible flame), and  $X = [1 + (1 + R_2^2/R_1^2)]$ . The symbols 1 and 2, respectively, refer to the transducer and the flame. Similarly, when the transducer was offset a distance  $a$  from the centerline, the relevant configuration factor was for a plane element with respect to a circular disk in a plane normal to the element, with the normal to the element now no longer passing through the disk center (Howell, 1982). The equation describing the factor is:

$$F_{1,2} = 0.5 [1 - (Z - 2R^2)/(Z^2 - 4R^2)^{1/2}] \quad (2)$$

where  $Z = 1 + H^2 + R^2$ , and  $H$  and  $R$ , respectively, were equal to  $(h/a)$  and  $(r_1/a)$ . In order to determine the value of  $h$ , the visible flame zone was taken to correspond to the peak temperature location (Yang et al., 1994).

### Radiative heat flux calculations

Three measurements, (at the centerline and at two off-center locations) were used to determine the radiative energy emitted through the top and bottom surfaces of the cylindrical control volume in the following manner:

$$Q_r = 2\pi \left( \oint_{A_{ox}} q_{ox}(r, z=0) r dr + \oint_{A_{fu}} q_{fu}(r, z=L) r dr \right) \quad (3)$$

The RHS of Eq. 3 represents the radiative flux emitted through the oxidizer duct and the fuel duct respectively. In Eq. 3,  $q$  is the measured heat flux at radial locations  $r$ ,  $A$  is the relevant control volume area, and the subscripts  $ox$  and  $fu$  refer to the oxidizer and fuel sides. Likewise, the radiative flux lost through the side of the control volume involves integration with respect to the axial direction:

$$Q_z = 2\pi R_3 \left( \int_0^{l_1} q_z(z) dz + \int_{l_1}^L q_z(z) dz \right) \quad (4)$$

where the two terms on the RHS represent the radiative energy emitted radially on fuel and oxidizer side of the visible flame. In Eq. 4,  $L$  denotes the separation between the two ducts,  $L_f$  the displacement of the flame from the oxidizer duct, and  $q_z$  the measured heat flux leaving the side of the cylindrical control volume at axial stations corresponding to a displacement  $z$ .  $R_3$  (= 60 mm) represents the radius of the cylindrical control volume. To perform the integration, polynomial fits were obtained for  $q_{ox}$  and  $q_{fu}$  versus  $r$ , and for  $q_z$  versus  $z$ .

### Global heat release

The integrated global heat release rate  $Q$  arising from within a stream tube is (Fristrom and Westenberg, 1965):

$$Q = \int_0^L q_n(z) A(z) dz \quad (5)$$

where  $q_n(z)$  denotes the local net heat release rate obtained from summing the heat release for each of the 358 chemical reactions in the simulation, and  $A(z)$  is the local stream tube area ratio. The value of  $A$  is based on the global continuity equation (Tsuji and Yamaoka, 1970), namely,

$$\rho v A = \rho_{ox/fu} v_{ox/fu} \quad (6)$$

In Eq. 6  $\rho$  denotes the density,  $v$  the velocity, and the subscripts  $ox$  and  $fu$  refer, respectively, to conditions at the oxidizer and fuel ducts.

## RESULTS AND DISCUSSION

The equilibrium heat release  $Q_e$  was calculated assuming a one-step reaction in which fuel and oxidizer react to form the products  $CO_2$  and  $H_2O$  in the case of methane, and  $CO_2$ ,  $H_2O$  and  $HCl$  in the case of chloromethane. The thermodynamic data for this calculation were obtained from Ref. (Chase et al., 1985). The equilibrium heat release rate was obtained on the basis of the oxidizer flowrate, since the overall stoichiometry was such that the flame was formed on the oxidizer side of the stagnation plane. The nonpremixed flame calculations were straightforward. For the flame inhibited with chloromethane on the oxidizer side, a lean premixed flame was first considered, followed by a nonpremixed flame. The amount of oxidizer associated with the two reaction zones differed, since a larger oxygen flowrate was available to the lean premixed flame than to the nonpremixed flame.

In Table 2 the equilibrium and global heat release rates from four flames are presented in the context of Eq. 5, as well as the integrated volumetric heat release rate calculated for a uniform stream tube (i.e.,  $A = 1$ ). Significant errors

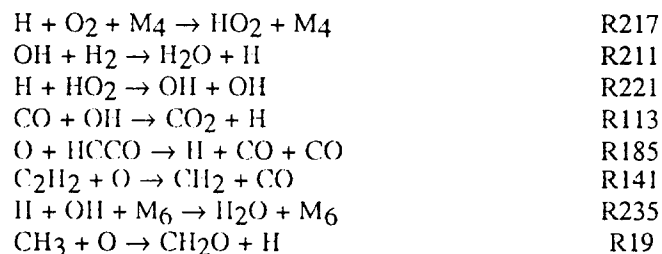
can arise if the value of  $A$  is miscalculated. Table 2 shows that the global heat release decreased as inhibitors were added to the oxidizer stream, but increased when chloromethane was added to the fuel stream of the nonpremixed flame.

Table 3 presents the spatially integrated net (sum of forward and backward) heat release rates integrated along the

axis of symmetry  $\int_0^L q(z) dz$  corresponding to the

significant exothermic reactions for flames with 13%  $N_2$  and 9%  $CH_3Cl$  added to the oxidizer stream, and for 50%  $CH_3Cl$  added to the fuel stream, where  $q$  denotes the local volumetric heat release rate. Consideration of the net heat release rates of key reactions allowed evaluation of the relative importance of a particular reaction pathway to flame energetics. For ease of presentation, discussion of a particular reaction refers to the net sum of the forward minus backward rates.

Addition of nitrogen inhibited the flames by decreasing the temperature and thereby diminishing the heat release due to reactions R217, R211, R221, R113, R185, R141, R235 and R19 (see Table 3).

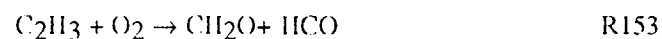


Though R113 and R211 had relatively large integrated heat release rates, both forward and backward rates involving these reactions were significant yielding a net rate that was not relatively significant.

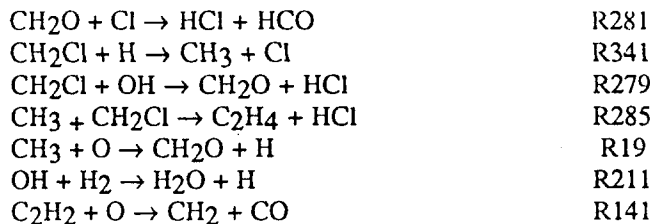
Table 3 shows that with the addition of 9%  $CH_3Cl$  to the oxidizer stream, the key reactions controlling the heat release were R299 and R305. Reaction R305 can be thought of as analogous to R211 in the base flame.



There were two distinct combustion regions in the flame established with the addition of 9%  $CH_3Cl$  to the oxidizer stream, namely, an oxidizer-side premixed type zone and a fuel-side nonpremixed type zone. Though the inhibitor was added to the oxidizer stream, reactions R299, R305, and R113 were dominant on the fuel side, whereas R153 was important on the oxidizer side of the flame.

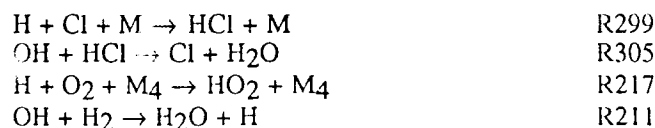


Reactions of secondary importance to the heat release included R281, R341, R279 and R285 with maxima in the premixed region, and R19, R211 and R141 in the nonpremixed region (in order of decreasing magnitude).

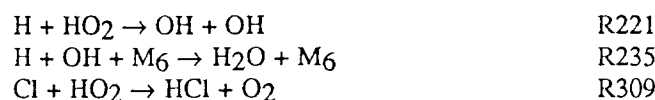


The net heat release associated with the *CO* burnout reaction (R113) rose, since *CO* is formed on both sides of the high temperature reaction zone. Chlorine is easily abstracted from chloromethane, and as a result *CH*<sub>3</sub> radicals were readily available for the formation of *C*<sub>2</sub> containing species (Lee et al., 1992). The increased role of the *C*<sub>2</sub> related chemistry was evident from the relative importance of R153 when *CH*<sub>3</sub>*Cl* was added to the oxidizer stream.

When chloromethane was added to the fuel stream the heat release due to R299 and R305 was larger than that due to reactions R217 and R211 which, though diminished, remained significant sources of heat release.

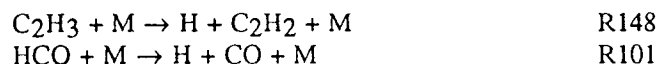
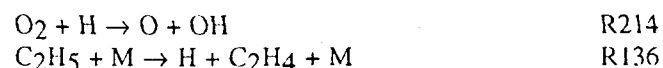


R221 and R235 were no longer significant whereas the heat release associated with *HO*<sub>2</sub> consumption occurred mainly through R309.



Thus, chlorine chemistry was of primary importance in terms of the heat release when chloromethane was added to the fuel stream (cf. R299 and R305) and the reactions associated with oxidation of methane took on a secondary importance (cf. R211, R217). Heat release due to the *CO* burnout reaction (R113) was not significantly perturbed by addition of chloromethane to the fuel stream.

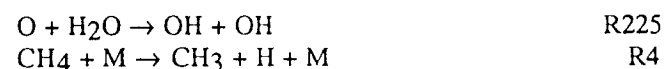
Table 4 contains a list of the significant endothermic reactions for a number of the flames. The important endothermic reactions in the base flame (in order of decreasing value) were R214, R136, R148, and R101, with the first three of the same order of magnitude.



Addition of nitrogen decreased the endothermicity, but not the ordering of the endothermic reactions. The same endothermic reactions were important when chloromethane was added to the flame, regardless of which side the addition occurred. Upon addition of 9% *CH*<sub>3</sub>*Cl* to the oxidizer stream the reactions R214, R136, R101, and R148 were still the key endothermic processes (listed in decreasing magnitude). There were no reactions involving chlorinated species that competed with these key reactions. Reaction R101 became a major channel for *CO* formation, since *O* atoms were depleted on the oxidizer side of the high temperature reaction zone, thereby suppressing the role of R185.



In addition, reactions R226 and R4 were key contributors to the endothermicity.



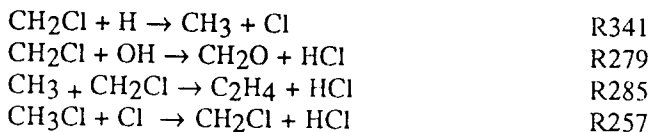
Endothermicity caused by addition of *CH*<sub>3</sub>*Cl* to the fuel stream was small, except for increased energy absorption due to R226, the reverse of reaction R225.



The global heat release profiles associated with the flames are presented in Fig. 3. Addition of nitrogen to the oxidizer stream narrowed the heat release region (consistent with the thermal suppression), though the nature of the profiles was qualitatively similar. Chloromethane addition to the fuel stream altered the flame stoichiometry, and moved the flame closer to the fuel duct. The heat release profiles were markedly different when *CH*<sub>3</sub>*Cl* was added to the oxidizer stream, with large amounts of heat release associated with the premixed flame. The heat release was considerably suppressed when the *CH*<sub>3</sub>*Cl* was raised to 9% by volume.

The smaller region over which the heat release took place in the presence of additional nitrogen lead to a lower net heat release, and thereby decreased the maximum flame temperature as shown in Fig. 4. Figure 4 also shows that chloromethane addition to the fuel stream slightly raised the peak flame temperature, and moved its location towards the fuel duct. The flame temperature profiles were broadened and the peak increased upon chloromethane addition to the oxidizer stream due to the additive enthalpy. The peak temperature location moved closer to the oxidizer duct when *CH*<sub>3</sub>*Cl* was added to that side in accord with the heat release distribution.

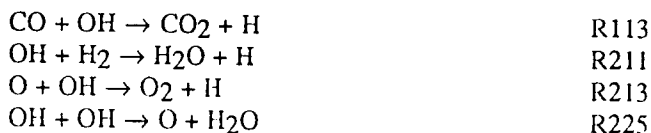
The impact of  $CH_3Cl$  addition on the heat release is illustrated in Figs. 5 and 6 where the profiles of significant exothermic reactions are presented. From these profiles it is noted that heat release on the oxidizer side of the flame occurred in a narrow region extending from  $\approx 5.3$  to  $\approx 5.8$  mm from the oxidizer duct. There, the chlorine chemistry impacted the heat release through reactions (in order of decreasing magnitude) R341, R279, R285, and R257.



Significant exothermic reactions that did not involve chlorine were the oxidative reactions R153 and R109. In a broad region extending from  $\approx 5.3$  to  $\approx 6.8$  mm the coupled reactions R299 and R305 dominated the heat release through transport of chlorine atoms to the flame. The result of the coupling was radical recombination through the net reaction (R299 + R305):



in which chlorine "catalyzed" chain termination. The exothermicity of the two reactions is also coupled through the  $CO$  burnout reaction R113. Chloromethane addition to the fuel stream did not exhibit as strong a coupling between reactions R299 and R305, since there were other competing exothermic pathways for  $OH$  consumption through R113, R211, R213, and R225.



## Radiation

Figure 7 shows the radiative heat flux measurements along  $R_3$  (the side) (see Fig. 2) for flames 1 and 5 of Table 2. The flux had a maximum near the duct center, where the highest flame temperatures occurred. The flux emitting from the side for a flame with 9% chloromethane added it on the oxidizer side was several times larger than that emitted by the base flame, as shown. Table 5 presents the measured radiative flux determined by summing Eqs. 3 and 4 for the five flames. The bulk of the thermal radiation was lost through the circular ducts rather than the sides of the cylindrical control volume. In general, the fuel-side duct accounted for a larger loss of radiative energy than does the oxidizer side. Calculations using RADCAL (Grosshandler, 1993) employing the simulated flame structure of the base flame substantiated the result that a higher radiative flux occurred towards the fuel duct than towards the oxidizer duct. This result can be attributed to

the larger concentrations of radiating gas species (primarily water vapor and carbon dioxide) on the fuel side of the high temperature reaction zone in accord with the results reported in Ref. (Hall, 1993).

In order to estimate the heat release, the global continuity equation must be applied separately to either side of the stagnation plane. The global heat release rate ( $Q_{n-A|e}$ ) due to the flame is (Fristrom and Westenberg, 1965):

$$Q_{n-A|e} = A_D \int_0^L q_n(z) A(z) dz \quad (7)$$

In Eq. 7  $q_n(z)$  denotes the local heat release rate obtained from Fig. 3,  $A_D$  is the duct area and  $A(z)$  was defined previously. Since most of the heat release occurred in the vicinity of the flame an approximate total heat release rate  $Q_{n-A|a}$  is obtained by multiplying the integrated axial heat release rate with the stream tube area at the flame location:

$$Q_{n-A|a} = A_D A_{st} \int_0^L q_n(z) dz \quad (8)$$

where the subscript  $st$  refers to the location of maximum temperature. In the context of Eqs. 7 and 8, the subscripts  $a$  and  $e$  refer respectively to the approximate and exact methods.

The diameter associated with the flame surface area calculated from Eq. 6 is much larger than the observed diameter of the visible flame (shown in Fig. 2) due to quenching of the flame edge by the curtain flow of nitrogen. Therefore, in order to estimate the total experimental heat release rate, the stream tube area ratio was assumed to attain a maximum value equal to the area corresponding to the surface of the visible flame  $A_{vf}$ , i.e.,  $A(z)$  was bounded between 1 and  $A_{vf}/A_D$ . Thus, the integrated heat release rate,  $Q_{n-vf|e}$ , corresponding to the experiment was obtained.

## Radiative emission

The stream tube area ratio at the location of maximum flame temperature, obtained by applying the global continuity equation is presented for the five flames in Table 6. Since the flame moved towards the oxidizer stream upon chloromethane addition, the velocity there was higher and the area ratio lower. The characteristic flame surface area was about 30% smaller for flame (5) when chloromethane was added as compared to flame (3) when nitrogen was added.

Table 6 also presents results for the heat release calculated using the methods described above. For all flames, the nonequilibrium heat release rate  $Q_{n-A|e}$  is

within 5% of that calculated assuming chemical equilibrium  $Q_{eq}$ . The approximate global heat release  $Q_{n-A|_e}$  calculated using Eq. 8 is as much as 15% larger than the heat release,  $Q_{n-A|_e}$ , calculated using Eq. 7. The approximation did somewhat better for flames near extinction (flames (3) and (5)). The heat release rate,  $Q_{n-vf|_e}$ , corresponding to the experiment is approximately a factor of 3 less than  $Q_{n-A|_e}$ , due to quenching of the flame edge by the nitrogen curtain.

Whichever method was used to calculate the heat release, addition of nitrogen decreased that value, primarily by decreasing the amount of oxygen available to the flame. Although the chloromethane flames (flames (4) and (5)) were closer to extinction, they had a higher heat release rate ( $Q_{n-vf|_e}$ ) than the uninhibited base flame (flame 1).

The fractional radiative loss from the flame  $\chi_R$  was determined by comparing the measured radiative flux with the total heat release rate based on  $Q_{n-vf|_e}$ . The  $\chi_R$  values so calculated are tabulated in Table 6. For the base case (flame 1),  $\chi_R$  is in good agreement with the value ( $= 0.02$ ) calculated in Ref. (Vranos and Hall, 1993) for moderately strained ( $100 \text{ s}^{-1}$ ) methane/air nonpremixed flames. As nitrogen was added to the oxidizer stream, the radiative heat loss fraction decreased slightly. This is consistent with the view that for flames near extinction, either through stretch or dilution with  $N_2$ , the radiative heat loss should diminish as the peak flame temperature decreases and the reaction zone narrows (Vranos and Hall, 1993, Chan et al., 1993). For flames to which a halogenated inhibitor was added to the oxidizer stream, the radiative emission increased (see Table 5) and so did the radiative heat loss fraction (Table 6).

In general, values of  $\chi_R$  do not differ much, taking on values from 2.0 to 3.5% for the five flames. This leads us to conclude that radiative losses do not significantly contribute towards extinction of *moderately* stretched flames, and that our simulations are reasonably accurate. However, analyses of extinguishment processes should consider radiation losses particularly if substantial amounts of particulates are present in the flames.

## CONCLUSIONS

The chemical and thermal structure of inhibited flames was investigated in order to characterize the effects due to inhibition on the heat release.

- In general, when inhibitors were added to the oxidizer stream of a nonpremixed flame, the global heat release decreased. However, chloromethane addition to the fuel stream increased the heat release. Whereas addition of nitrogen narrowed the heat release region, chloromethane addition to the oxidizer altered the flame structure, such that two distinct heat release regions were present.

- Halogen addition to the oxidizer stream of flames introduced substitute pathways to supplement those by which the heat release occurred (e.g., R299 and R305 in addition to R217 and R211). Though inhibition effects occurred in a premixed-like region on the oxidizer side of the high temperature reaction zone, the effects of mass diffusion and thermochemistry were such that halogen-involving heat release reactions were dominant on the fuel side.
- Compared to the chemistry associated with hydrocarbon burning, halogenated channels were the dominant heat release paths when chloromethane was added to the fuel stream. Furthermore, the *CO* burnout reaction was not significantly perturbed by addition of chloromethane to the fuel stream of the base flame.
- Halogen addition to either side of the flame did not significantly affect the endothermic pathways.
- Chloromethane addition to the oxidizer resulted in a coupling of the premixed and nonpremixed flame regions through the net reaction  $H + OH + Cl \rightarrow H_2O + Cl$ .
- Radiative heat flux measurements obtained in moderately strained counterflow diffusion flames showed that:
  - As nitrogen was added to the "base" flame, the radiative heat loss fraction decreased somewhat (<20%), whereas when a halogenated inhibitor was added to that flame, the radiative heat loss fraction increased substantially (>80%).
  - The fractional radiative flux emitted from these moderately strained flames was very small in comparison with the total flame heat release and the radiative flux did not significantly contribute towards flame extinction. Thus, numerical simulations of flame structure can reasonably neglect emission from such moderately strained flamelets.

## ACKNOWLEDGMENTS

The authors thank Dr. M. H. Yang of UIC for several helpful discussions.

## REFERENCES

- Abdel-Khalik, S., Tamaru, T. and El-Wakil, M. M., 1974, Chapter 23 in Heat Transfer in Flames, N. H. Afgan and J. M. Beer Eds., Scripta Book Co, Washington D.C.
- Barat, R. B., Sarofim, A. F., Longwell, J. P. and Bozzelli, J. W., 1990, *Combustion Science and Technology*, Vol. 74, pp. 361-378.
- Chan, S. H., Pan, X. C. and Abou-Elail, M. M. M., 1993, "Radiative Flamelet Modeling of Nonpremixed - Air Flames," Presented at the Presented at the Eastern States



- Section Meeting of the Combustion Institute held at Princeton, NJ, October 25-27.
- Chang, W. D., Karra, S. B. and Senkan, S. M., 1987, *Combustion and Flame*, Vol. 69, pp.113-122.
- Chase, M. W., Davies, C. A., Downey, J. R., Frurip, D. J., MacDonald, R. A. and Syverud, A. N., 1985, JANAF Thermochemical Tables, Third Edition. ACS and AIP for NBS, 14.
- Chelliah, H. K., Law, C. K., Ueda, T., Smooke, M. D. and Williams, F. A., 1990, Twenty-third Symposium (International) on Combustion, The Combustion Institute, pp. 503-511.
- Dixon-Lewis, G., David, T., Gaskell, P. H., Fukutani, S., Jinno, H., Miller, J. A., Kee, R. J., Smooke, M. D., Peters, N., Effelsburg, E., Warnatz, J. and Behrendt, F., 1984, Twentieth Symposium (International) on Combustion, The Combustion Institute, pp. 1893-1904.
- Fristrom, R. M. and Westenberg, A. A., 1965, "Flame Structure," McGraw-Hill, New York.
- Grosshandler, W. L., 1993, "RADCAL: A narrow-band model for radiation calculations in a combustion environment," U.S. Government Printing Office - NIST Publication 1402.
- Hall, R. J., 1993, *Journal of Quantitative Spectroscopy & Radiative Transfer*, Vol. 49, pp.517-523.
- Hamins, A., Thridandam, H. and Seshadri, K., 1985, *Chemical Engineering Science*, Vol. 40, pp. 2027-2038.
- Hamins, A., Klassen, M., Gore, J. and Kashiwagi, T., 1991, *Combustion and Flame*, Vol. 86, pp. 223-228.
- Howell, J. R., 1982, "A Catalog of Radiation Configuration Factors," McGraw-Hill, New York, pp. 32-33.
- Huh, J. Y., Lee, K. Y. and Puri, I. K., 1994, *Combustion and Flame*, Vol. 86, pp. 381-392.
- Karra, B., Gutman, D. and Senkan, S. M., 1988, *Combustion Science and Technology*, Vol. 60, pp. 45-62.
- Lee, K. Y., Yang, M. H. and Puri, I. K., 1992, *Combustion and Flame*, Vol. 92, pp 419-439.
- McCaffrey, B. J., 1981, "Some measurements of the radiative power output of diffusion flames," Presented at the Meeting of the Western States Section of the Combustion Institute held at 1981.
- Miller, J. A. and Bowman, C. T., 1989, *Progress in Energy and Combustion Science*, Vol. 15, pp. 287-338.
- Pitz, W. J. and Westbrook, C. K., 1990, "Chemical kinetic modeling of chlorinated hydrocarbons under stirred-reactor conditions," Presented at the Western States Section/ The Combustion Institute held at La Jolla, California.
- Puri, I. K., 1987, "The structure and extinction of counterflow flames," Ph.D. Thesis, University of California, San Diego.
- Rogg, B., 1989, "Computers and Experiments in Fluid Flow," G. M. Carlomagno and C. A. Brebbia Eds., Springer Verlag, Berlin, pp. 75-85.
- Rogg, B., 1991, "RUN-1DS: A computer program for the simulation of one-dimensional chemically reacting flows," University of Cambridge, April, 1991. Report CUED/A-THERMO/TR39.
- Smooke, M. D. and Giovangigli, V., 1991, "Reduced Kinetic Mechanisms and Asymptotic Approximations for Methane-Air Flames," M. D. Smooke Ed., Springer Verlag, Berlin, pp. 1-28.
- Sohrab, S. H., Linan, A. and Williams, F. A., 1982, *Combustion Science and Technology*, Vol. 27, pp. 143-154.
- Tsuji, H. and Yamaoka, I., 1970, Thirteenth Symposium (International) on Combustion, The Combustion Institute, pp. 723-731.
- Vranos, A. and Hall, R. J., 1993, *Combustion and Flame*, Vol. 93, pp 230-238.
- Williams, F. A., 1985, "Combustion Theory," Benjamin/Cummings, Menlo Park, California.
- Yang, M. H. and Puri, I. K., 1993, *Combustion and Flame*, Vol. 94, pp 25-34.
- Yang, M. H., Hamins, A. and Puri, I. K., 1994, *Combustion and Flame*, Vol. 98, pp. 107-122.

Table 1: The flow and measurement conditions for the five different flames that are studied. The fuel duct velocity is denoted by  $V_F$  and the oxidizer duct velocity by  $V_O$ , and  $O$  and  $F$  respectively denote the oxidizer and fuel sides. The measurement condition refers to either of Case I or II referred to in the text.

Flame	$V_F$ m s <sup>-1</sup>	$V_O$ m s <sup>-1</sup>	Centerline		Off-center	
			O	F	O	F
			1) CH <sub>4</sub> -Air	0.74	0.68	I
2) + 6.6% N <sub>2</sub>	0.74	0.70	I	II	I	II
3) + 13% N <sub>2</sub>	0.74	0.72	I	II	I	II
4) + 5% CH <sub>3</sub> Cl	0.76	0.65	I	II	I	II
5) + 9% CH <sub>3</sub> Cl	0.77	0.63	I	II	I	II

Table 2: The equilibrium, global heat release rates, and integrated volumetric heat release rates calculated for a uniform stream tube ratio.

Flame	added to	$Q_{eq}$ W m <sup>-2</sup>	$Q$ W m <sup>-2</sup>	$\int q_v dz$ W m <sup>-2</sup>
1) CH <sub>4</sub> -Air	-	2.39·10 <sup>6</sup>	2.51·10 <sup>6</sup>	2.68·10 <sup>5</sup>
2) + 6.6% N <sub>2</sub>	oxidizer	2.29·10 <sup>6</sup>	2.40·10 <sup>6</sup>	2.55·10 <sup>5</sup>
3) + 13% N <sub>2</sub>	oxidizer	2.11·10 <sup>6</sup>	2.27·10 <sup>6</sup>	2.42·10 <sup>5</sup>
4) + 5% CH <sub>3</sub> Cl	oxidizer	2.22·10 <sup>6</sup>	2.21·10 <sup>6</sup>	3.03·10 <sup>5</sup>
5) + 9% CH <sub>3</sub> Cl	oxidizer	2.12·10 <sup>6</sup>	1.19·10 <sup>6</sup>	3.34·10 <sup>5</sup>
6) + 50% CH <sub>3</sub> Cl	fuel	2.57·10 <sup>6</sup>	3.04·10 <sup>6</sup>	2.42·10 <sup>5</sup>

Table 3: Significant net heat release rates associated with *exothermic* reactions in units of J s<sup>-1</sup> m<sup>-2</sup>. The symbol \* signifies a heat release rate that is less than 10<sup>3</sup> J s<sup>-1</sup> m<sup>-2</sup>.

		Base flame	+13% N <sub>2</sub>	+9% CH <sub>3</sub> Cl	+50% CH <sub>3</sub> Cl
(R19)	CH <sub>3</sub> + O → CH <sub>2</sub> O + H	-1.20·10 <sup>4</sup>	-1.29·10 <sup>4</sup>	-1.75·10 <sup>4</sup>	-8.62·10 <sup>3</sup>
(R113,114)	CO + OH = CO <sub>2</sub> + H	-2.29·10 <sup>4</sup>	-2.14·10 <sup>4</sup>	-3.26·10 <sup>4</sup>	-2.31·10 <sup>4</sup>
(R141)	C <sub>2</sub> H <sub>2</sub> + O → CH <sub>2</sub> + CO	-1.74·10 <sup>4</sup>	-1.42·10 <sup>4</sup>	-1.03·10 <sup>4</sup>	-1.34·10 <sup>4</sup>
(R153)	C <sub>2</sub> H <sub>3</sub> + O <sub>2</sub> → CH <sub>2</sub> O + HCO	*	*	-2.05·10 <sup>4</sup>	*
(R185)	O + HCCO → H + CO + CO	-2.01·10 <sup>4</sup>	-1.67·10 <sup>4</sup>	*	-1.62·10 <sup>4</sup>
(R211,212)	OH + H <sub>2</sub> = H <sub>2</sub> O + H	-3.81·10 <sup>4</sup>	-3.33·10 <sup>4</sup>	-1.35·10 <sup>4</sup>	-1.97·10 <sup>4</sup>
(R217)	H + O <sub>2</sub> + M <sub>4</sub> → HO <sub>2</sub> + M <sub>4</sub>	-5.87·10 <sup>4</sup>	-4.76·10 <sup>4</sup>	*	-1.94·10 <sup>4</sup>
(R221)	H + HO <sub>2</sub> → OH + OH	-2.94·10 <sup>4</sup>	-2.52·10 <sup>4</sup>	*	*
(R235)	H + OH + M <sub>6</sub> → H <sub>2</sub> O + M <sub>6</sub>	-1.59·10 <sup>4</sup>	*	*	*
Cl-related chemistry					
(R257,258)	CH <sub>3</sub> Cl + Cl = CH <sub>2</sub> Cl + HCl	*	*	-8.00·10 <sup>3</sup>	*
(R259)	CH <sub>3</sub> Cl + H → CH <sub>3</sub> + HCl	*	*	*	-5.49·10 <sup>3</sup>
(R279)	CH <sub>2</sub> Cl + OH → CH <sub>2</sub> O + HCl	*	*	-1.52·10 <sup>4</sup>	*
(R281)	CH <sub>2</sub> O + Cl → HCO + HCl	*	*	-1.68·10 <sup>4</sup>	*
(R285)	CH <sub>3</sub> + CH <sub>2</sub> Cl → C <sub>2</sub> H <sub>4</sub> + HCl	*	*	-1.01·10 <sup>4</sup>	*
(R299)	H + Cl + M → HCl + M	*	*	-1.15·10 <sup>5</sup>	-8.21·10 <sup>4</sup>
(R305,306)	OH + HCl = Cl + H <sub>2</sub> O	*	*	-4.53·10 <sup>4</sup>	-2.30·10 <sup>4</sup>
(R309)	Cl + HO <sub>2</sub> → HCl + O <sub>2</sub>	*	*	*	-9.74·10 <sup>3</sup>
(R341)	CH <sub>2</sub> Cl + H → CH <sub>3</sub> + Cl	*	*	-1.58·10 <sup>4</sup>	*

Table 4: Significant net heat release rates associated with *endothermic* reactions in units of J s<sup>-1</sup> m<sup>-2</sup>. The symbol \* signifies a heat release rate that is less than 10<sup>3</sup> J s<sup>-1</sup> m<sup>-2</sup>.

		Base flame	+13% N <sub>2</sub>	+9% CH <sub>3</sub> Cl	+50% CH <sub>3</sub> Cl
(R4)	CH <sub>4</sub> + M <sub>1</sub> → CH <sub>3</sub> + H + M <sub>1</sub>	*	*	1.02·10 <sup>4</sup>	*
(R101)	HCO + M <sub>2</sub> → H + CO + M <sub>2</sub>	1.23·10 <sup>4</sup>	1.05·10 <sup>4</sup>	2.88·10 <sup>4</sup>	1.14·10 <sup>4</sup>
(R133,136)	H + C <sub>2</sub> H <sub>4</sub> + M <sub>1</sub> = C <sub>2</sub> H <sub>5</sub> + M <sub>1</sub>	3.38·10 <sup>4</sup>	2.83·10 <sup>4</sup>	3.05·10 <sup>4</sup>	2.84·10 <sup>4</sup>
(R148)	C <sub>2</sub> H <sub>3</sub> + M <sub>1</sub> → H + C <sub>2</sub> H <sub>2</sub> + M <sub>1</sub>	2.98·10 <sup>4</sup>	2.39·10 <sup>4</sup>	2.15·10 <sup>4</sup>	2.27·10 <sup>4</sup>
(R213,214)	O + OH = O <sub>2</sub> + H	3.45·10 <sup>4</sup>	2.96·10 <sup>4</sup>	4.66·10 <sup>4</sup>	3.64·10 <sup>4</sup>
(R223,226)	OH + OH = O + H <sub>2</sub> O	4.75·10 <sup>3</sup>	4.59·10 <sup>3</sup>	1.86·10 <sup>4</sup>	1.24·10 <sup>4</sup>
Cl-related chemistry					
(R251)	CH <sub>3</sub> Cl → CH <sub>3</sub> + Cl	*	*	*	1.22·10 <sup>4</sup>

Table 5: The measured emitted heat flux calculated by summing Eqs. 3 and 4 for some flames.

Flame	Measured Radiative Flux (W)				
	Oxidizer side		Fuel side		Total
	Radial	Axial	Radial	Axial	
1) CH <sub>4</sub> -Air	10.8	2.7	17.3	3.0	33.8
2) + 6.6% N <sub>2</sub>	9.8	2.4	13.9	2.6	28.7
3) + 13% N <sub>2</sub>	9.6	2.2	11.2	2.5	25.5
4) + 5% CH <sub>3</sub> Cl	14.8	3.2	21.3	4.2	43.5
5) + 9% CH <sub>3</sub> Cl	23.1	4.7	27.7	6.0	61.5

Table 6: The stream tube area ratio  $A$  at the maximum flame temperature, displacement of the peak temperature location from the oxidizer duct  $L_I$ , heat release based on (a) chemical equilibrium  $Q_{eq}$ , (b) the numerical simulations and the stream tube area  $Q_{n-A}$ , and (c) the numerical simulations and the visible flame area  $Q_{n-vf}$  (the subscripts  $-e$  and  $-a$  refer to the exact and approximate methods discussed in the text), and the fractional radiative flux  $c_R$  based on  $Q_{n-vf}/e$  expressed in percent.

Flame	$A_m$	$L_I$ mm	Heat release (W)				$X_R$
			$Q_{eq}$	$Q_{n-A,e}$	$Q_{n-A,a}$	$Q_{n-vf,e}$	
1) CH <sub>4</sub> -Air	10.5	7.3	4330	4550	5090	1420	2.4
2) + 6.6% N <sub>2</sub>	10.5	7.3	4150	4340	4830	1350	2.1
3) + 13% N <sub>2</sub>	10.4	7.3	3810	4100	4530	1280	2.0
4) + 5% CH <sub>3</sub> Cl	8.5	6.9	4020	4010	4640	1600	2.7
5) + 9% CH <sub>3</sub> Cl	6.9	6.5	3840	3600	4180	1770	3.5

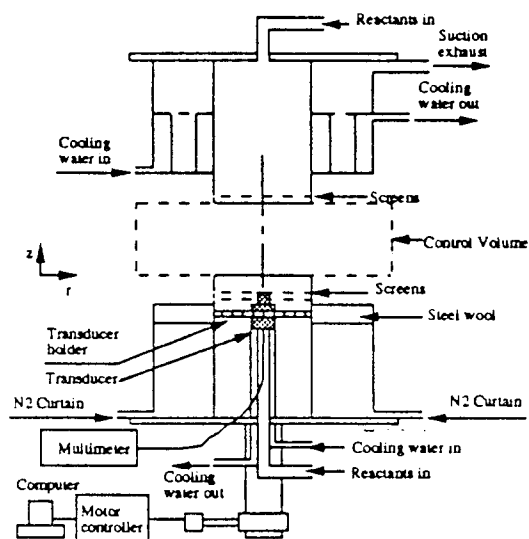


Figure 1. Schematic diagram of the burner and measurement assembly. The drawing is not to scale.

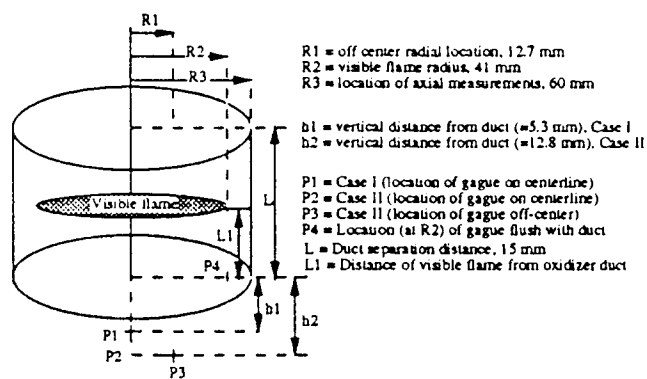


Figure 2. Schematic diagram of the control volume employed to make measurements of the radiative flux. The measurement locations corresponding to Case I and Case II are also shown.

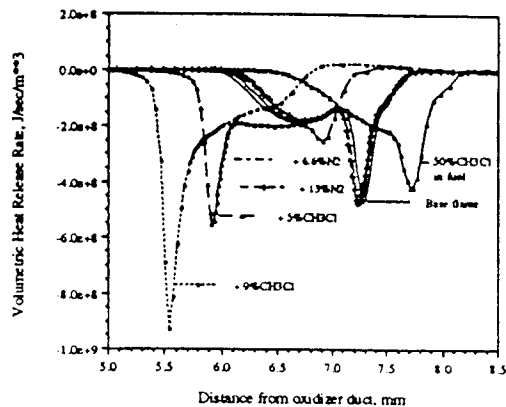


Figure 3: The heat release profiles of several flames.

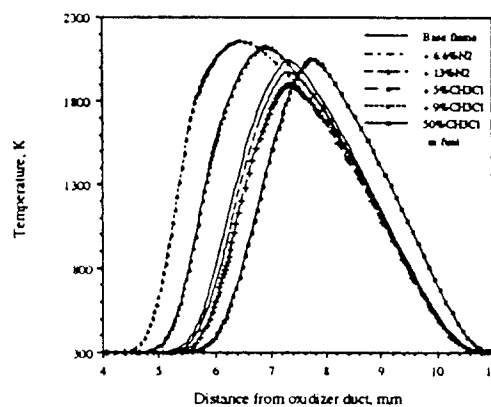


Figure 4: The temperature profiles of several flames.

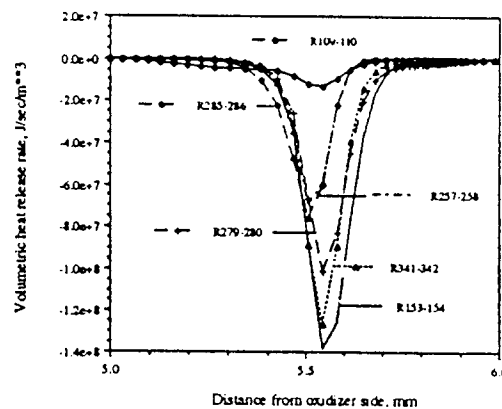


Figure 5: The heat release profiles of some significant exothermic reactions in flame (5) (see Table 2).

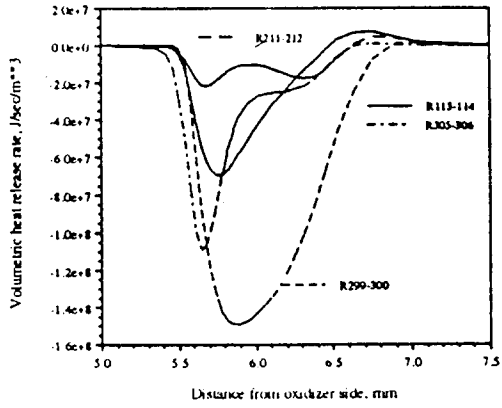


Figure 6: The heat release profiles of other significant exothermic reactions in flame (5) (see Table 2).

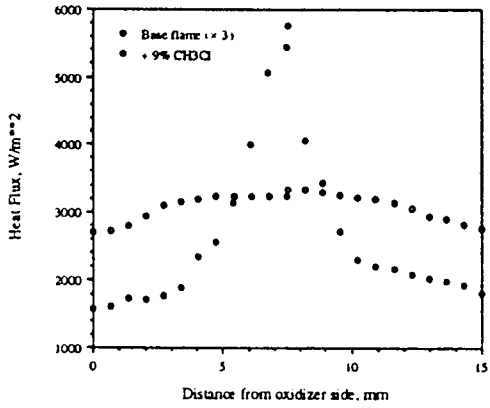


Figure 7: The measured radiative heat flux profiles measured along R3 (see Fig. 2).